High Q ultra-low threshold lasing in conjugated polymer blend microspheres promoted by FRET

Jorge González Sierra, Alejandro Martin-Merinero, Javier Álvarez-Conde, Sergio Iglesias Vázquez, Juan Cabanillas-González*, Reinhold Wannemacher*

High Q ultra-low threshold lasing in conjugated polymer blend microspheres promoted by FRET

Jorge González Sierra, Alejandro Martin-Merinero, Javier Álvarez-Conde, Sergio Iglesias Vázquez, Juan Cabanillas-González; Reinhold Wannemacher**

Madrid Institute for Advanced Studies, IMDEA Nanociencia, c/ Faraday, 9, Ciudad Universitaria de Cantoblanco, Madrid 28049, Spain

AUTHOR INFORMATION

Corresponding Authors

Juan Cabanillas-González

IMDEA Nanoscience

C/ Faraday 9, Cantoblanco, Madrid 28049, Spain

E-mail: juan.cabanillas@imdea.org

Reinhold Wannemacher

IMDEA Nanoscience

C/ Faraday 9, Cantoblanco, Madrid 28049, Spain

E-mail: reinhold.wannemacher@imdea.org

Keywords: Conjugated Polymers, polymer blends, FRET, microspheres, lasing

Conjugated polymer (CP) based microspheres of very high definition and outstanding photonic and luminescent properties are prepared by a technique based on slow solvent-controlled diffusion into micelles formed by the surfactant cetyl(trimethyl)ammonium bromide (CTAB), Poly[(9,9-di-*n*-octylfluorenyl-2,7-diyl)-*alt*-(benzo[2,1,3]thiadiazol-4,8-diyl)] (F8BT) and mixtures of F8BT with poly[2-methoxy-5-(2'-ethylhexyloxy)-1,4-phenylene vinylene (MEH-PPV) are used for this purpose. Microspheres with diameters between 1 and 10 μm are obtained and

structural characterization by AFM and SEM demonstrate good sphericity and low surface roughness. Correspondingly, spontaneous emission of the spheres exhibits Mie resonances of high quality factor (Q > 1800), appropriately reproduced employing standard Mie theory. Upon pumping the microspheres with a pulsed Nd:YAG laser operating at 355 nm we obtain lasing at low threshold fluences (≈ 4 μJ/cm^2) with instrumentally limited linewidths corresponding to Q > 18000. Lasing in microspheres composed of blends of both CPs coupled by Förster resonant energy transfer (FRET), on the other hand, is observed at extremely low threshold fluences down to ≈ 0.5 μJ/cm^2. The observed lasing thresholds are lower and the observed Q factors higher than those reported previously for the CPs considered here. Spherical structures based on appropriate blends of CPs are therefore promising candidates in the search for low-threshold organic microlasers excited by light-emitting diodes or diode lasers or for ultrasensitive optical sensing.

1. Introduction

Dielectric optical microresonators offer the possibility to achieve control of light confinement and propagation through precise adjustment of their shape, size and refractive index. Among them, spherical mode resonators are particularly interesting due to the typically high Q factors, Q > 10^8 in some inorganic microspheres,[1,2] of the corresponding Mie resonances (often generically termed “whispering gallery modes”, although this term should be reserved to Mie resonances with azimuthal quantum number m equal to the angular momentum l, see **Figure S1** and compare, for example [3]). In a geometrical optics perspective, these Q factors stem from multiple near total internal reflections at the curved dielectric-air interface leading to closed loops where light interferes constructively for certain wavelengths. The resulting narrow resonances enable applications in the optical sensing field, including chemical,[4–7] biological or physical sensors with high sensitivity to small physical or chemical variations in the optical near field of the spheres.[8–14] Related to the high Q factors is the high optical power density

inside the spheres, which paves the way for quantum- optical applications,[15–17] via enhancement of light-matter interactions. Also, high Q factors pave the way for applications in nonlinear optics,[18,19] or in the field of amplified spontaneous emission (ASE) and lasing of microspheres made of luminescent materials or coated with luminescent materials,[20–23] such as organic dyes or quantum dots.[16,17,24–27] ASE and lasing give raise to strong linewidth narrowing that can be favorably employed for sensing with enhanced sensitivities. Table S1 provides an overview of some recent results concerning Q factors and lasing thresholds of organic microspheres and demonstrates an improvement in both figures of merit by the present work.

Microlasers with different resonator geometries such as rings,[28,29] toroids or spheres based on luminescent organic dyes or conjugated polymers (CPs) have been reported,[30–32] with typical Q factors in the 10^3 range. These observations have indeed prompted applications of these microlasers as highly sensitive sensors as well as for labelling and tracking cells in a biological medium.[8,33–35] Although organic dyes have been widely exploited as optical gain medium, their tendency to aggregate typically imposes restrictions on the maximum useful dye concentration inside solid-state microlasers, limiting in this way the overall absorption of the microresonator and consequently its emitted light intensity upon optical pumping.

In recent years, microspheres exhibiting Mie resonances based on luminescent conjugated polymers (CPs) obtained by simple self–assembly methods were demonstrated.[7,20,35–42] In contrast to organic dyes, the highly disordered nature of CPs is key to induce steric hindrance in solid state and curtail strong π-π interactions, which would otherwise compromise their luminescence properties.[43–48] Accordingly, CP microspheres combine large optical absorption with high photoluminescence (PL) quantum yields, affording an order of magnitude increase of brightness with respect to commercial dye-doped microspheres under the same photoexcitation conditions, as well as lower pumping thresholds for lasing.[20] In an exceptional case,[36] Mie resonances in the PL spectrum of such CP microspheres with a Q factor of about

4000, before correction for the instrumental resolution, were obtained, although lasing of the microspheres was not reported in that particular case.

CP self-organization into microspheres typically requires the use of an anti-solvent diffusing slowly into a CP solution to induce chain coiling and particle precipitation. Vapor diffusion can lead to well defined microspheres with smooth surfaces, provided that the CP backbone is sufficiently pliable, which otherwise leads to surface inhomogeneity and loss of sphericity.[38,42] An alternative method which can be extended to a wider range of CPs involves their dispersion in microemulsions. For this purpose, a volume of CP solution is dispersed in water containing a surfactant. Subsequent emulsification leads to micelles whose inner hydrophobic core enables CP to self-assemble inside them.[7,21,23,38] The resultant microspheres are capped by the surfactant, which can be subsequently released from the surface upon successive washing and centrifugation cycles. This method allows, for instance, the processing of the yellow emitting poly(9,9-dioctylfluorene-alt-benzothiadiazole) (F8BT), a CP exhibiting notable optical gain properties,[49–52] into microspheres of 2 - 10 µm with maximum reported Q factors of $1.5 \cdot 10^3$ under lasing conditions.[7,38]

In the quest for efficient CP lasers, the use of host:guest blends coupled by Förster resonance energy transfer (FRET) have proved in the past to be effective in boosting the stimulated emission property, due to reduction of self-absorption,[53–57] caused by spectral displacement of the guest emission from the host absorption, and PL quantum yield enhancement arising from guest CP dilution in the host matrix. Such blends were also previously exploited as a way to widely tune microsphere emission through control of the CP host:guest ratio and to induce long-range radiative energy transfer between spheres.[32,39,58] Whereas FRET between host and guest CPs inside a microsphere and sharp Mie resonances have been reported for such blends previously,[32] the effect of CP guest doping on the lasing properties of CP microspheres has so far remained unaddressed. In this work we report on CP microspheres based on F8BT, doped

at different concentrations with poly [2-methoxy-5- (2'-ethylhexyloxy)-1,4-phenylene vinylene] (MEH-PPV), a red emitting CP (**Figure S2**).

2. Results and Discussion

2.1. Morphological Characterization

Figure 1(a-d) displays SEM images of microspheres of F8BT and mixtures of MEH-PPV in F8BT in different weight ratios (15%, 10% and 5%, respectively). Excellent sphericity was evident in all cases. AFM maps of their surface, after compensation for the spherical curvature, demonstrate roughnesses in the range of a few nm (**Figure 1(e,f)**). This roughness appears to

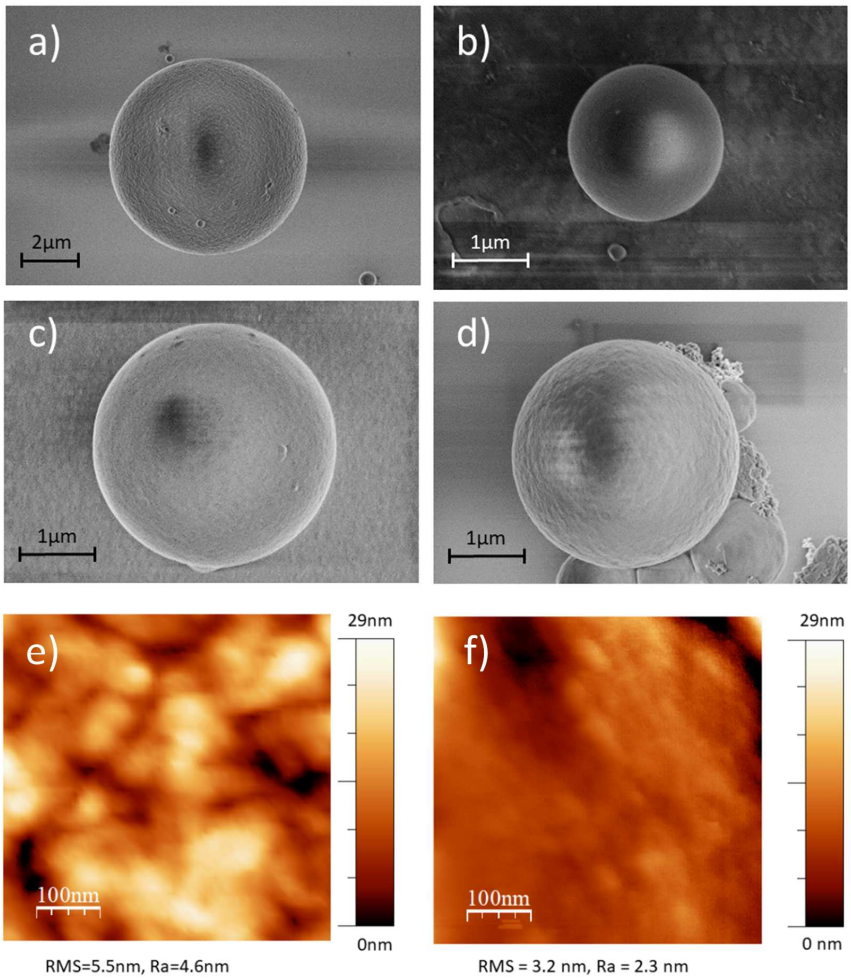

Figure 1. SEM images of microspheres of a) F8BT and of blends of MEH-PPV in F8BT in different ratios b) 15%, c) 10% and d) 5%. (e,f) AFM maps of the surface of microspheres based on e) F8BT and f) 10% blends. Area 500x500 nm^2. Spherical curvature is subtracted. RMS: root mean square roughness, Ra: average roughness.

be larger for microspheres made from pure F8BT than for the blends. Statistical parameters of the size distribution of the microspheres produced were determined from 30 microspheres of each composition (**Figure 2**). Mean values/standard deviations of their diameters were evaluated to be 2.9/1.0 μm (F8BT), 4.8/2.1 μm (15%), 3.1/1.1 μm (10%) and 2.1/1.0 μm (5%) respectively.

2.2.

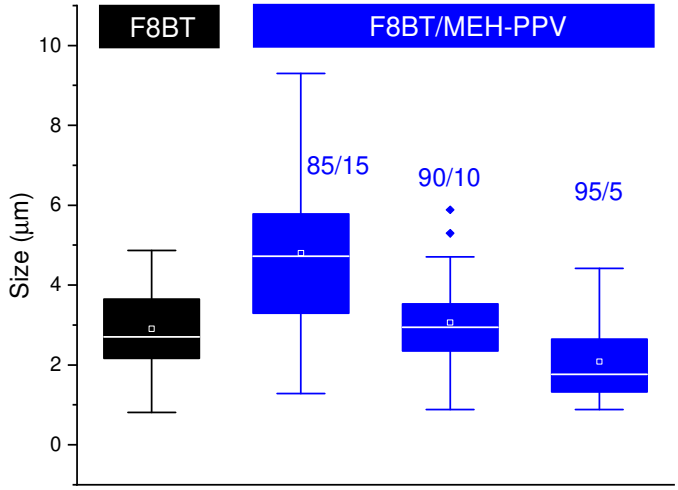

Figure 2. Statistical parameters of the size distribution of microspheres produced from F8BT and different blends of F8BT and MEH-PPV obtained upon sampling 30 microspheres of each type. The bars show the interquartile ranges Q1 and Q4. The boxes correspond to the interquartile ranges Q2 and Q3, the white line being the median and the white dot the mean. The outer points are outliers. 30 microspheres were used for statistical analysis in each case.

Microspectroscopy of CP Microspheres

Spontaneously emitted PL spectra of individual microspheres under continuous wave photo-excitation are shown in **Figure 3**. Serving as examples are spheres of different diameters and MEH-PPV weight percentage: 1.50 μm (15%), d =3.72 μm (10%), 3.97 μm (5%) and 2.67 μm (F8BT), (**Figure 3(a-d),** respectively). The sphere diameters were extracted from the corresponding camera images (shown in the figure insets), with an error of about ±0.05 μm (estimated from the blur of the diffraction-limited image). As expected, a gradual spectral shift

is found upon doping the microspheres with MEH-PPV. Whereas the absorption and excitation spectra of the mixtures (**Figures S2** and **S3**) are dominated by the absorption of F8BT, the emission spectra are clearly dominated by the PL of MEH-PPV, even for the lowest concentration of 5% MEH-PPV in the mixture. This demonstrates that there is no independent emission from the two CPs, but photoexcitation of F8BT is followed by energy transfer to MEH-PPV. Time-resolved single photon counting experiments (**Figure S5**) demonstrate that the PL lifetime of F8BT in the blends is significantly shortened compared to pure F8BT, which again indicates that the transfer is due to FRET and, hence, non-radiative.

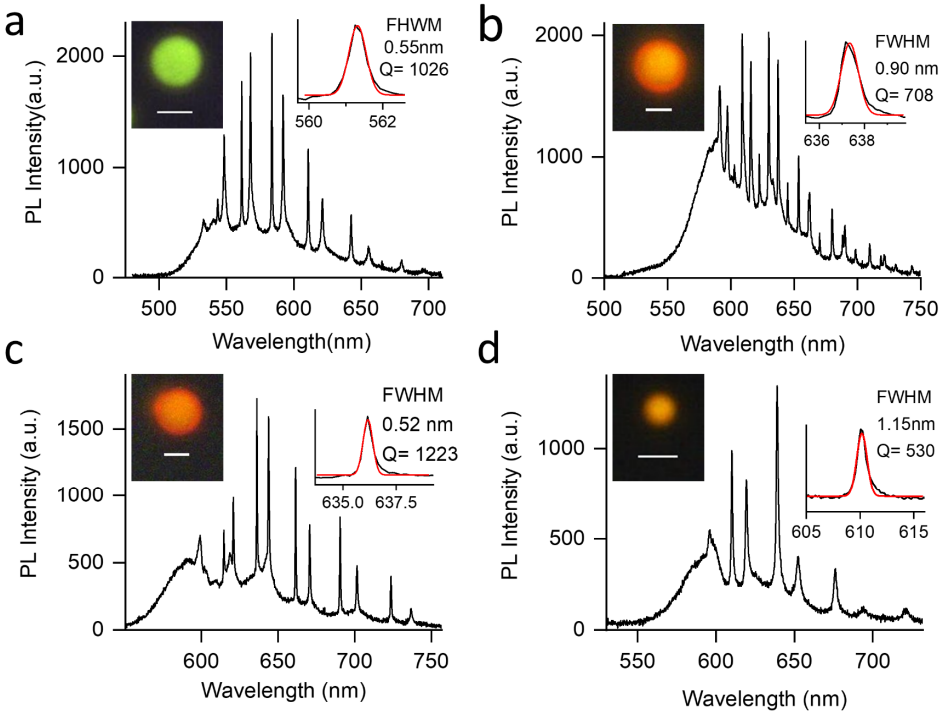

Figure 3. Spontaneous emission spectra of individual CP microspheres of a) pure F8BT b) 5%, c) 10%, d) 15% MEH-PPV in F8BT. Microscope camera images of the spheres are shown with scale bars of 2 µm. Sphere diameters determined from the images are a) 2.80 µm, b) 3.74 µm, c) 3.61 µm and d) 1.33 µm, with an error of approximately ±0.05 µm. The excitation wavelength was 355 nm. The graphs in the insets represent the spectra expanded in the vicinity of a selected Mie resonance together with a Gaussian fit and corresponding quality factors, without correction for the instrumental linewidth.

In contrast to the PL spectra of spin-cast blend films (**Figure S4**) PL from blend-based microspheres exhibit high amplitude Mie resonances and high Q factors favored by the excellent sphericity and low surface roughness. For the spheres shown in **Figure 3**, Q factors of 1026, 708, 1223 and 530 were inferred for F8BT, 5%, 10% and 15% respectively from Gaussian fits of the selected sphere resonances. Employing a Gaussian deconvolution to correct for the instrumental contribution, Q values of 1435, 784, 1833 and 565 were respectively obtained. These values significantly exceed the spontaneous emission Q factors ($Q \approx 300$) previously reported for F8BT microspheres and are equivalent to much stronger Mie resonances compared to this previous report.[7]

It should be remarked here that attempts to fabricate microspheres from pure MEH-PPV in many cases resulted in large holey microspheres (**Figure S6**) which did not exhibit Mie resonances in their PL spectra, an effect which we ascribe to high polymer molecular weight, in line with previous reports.[20,59] However, such resonances were finally observed upon adjustment of the fabrication parameters (see **Figure S7**), albeit with significantly smaller Q values than microspheres produced from the blends or from pure F8BT.

2.3. Simulation by standard Mie theory

Microsphere resonances are of transverse electric (TE) and transverse magnetic (TM) character and can be modeled following standard Mie theory. The sphere size is obtained from images acquired with the microscope camera and the real part of the refractive index follows from ellipsometric data acquired on thin films of the corresponding CP.[60] The imaginary part of the refractive index in the region of transparency of the CPs is too small to be reliably determined by ellipsometry and is set to zero in the simulation.

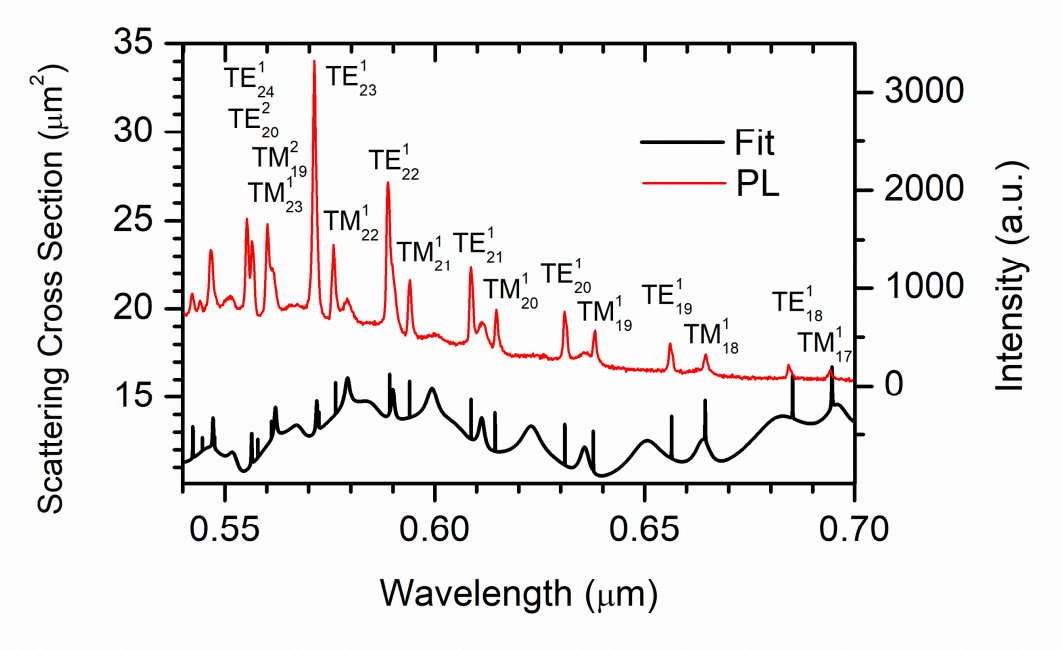

Figure 4. PL spectrum of a particular F8BT microsphere and a fit according to standard Mie theory (d = 2.7 μm).

Taking into account the size of a particular sphere and the refractive index of the CP and surrounding medium, the spectral position of the TE and TM modes can be modeled by calculating the scattering cross section of the sphere. **Figure 4** shows, as an example, a comparison between the PL spectrum of a given F8BT microsphere of 2.70 μm diameter and its corresponding fit employing standard Mie theory, assuming a diameter of 2.674 μm. To achieve excellent agreement required the use of a wavelength-dependent refractive index correction function which gradually reduces the real part of the refractive index by 2% towards the short wavelength limit of the spectrum, λ=0.54 μm (**Figure S8**). This is not surprising because the refractive index of the thin film may slightly vary from that of the microsphere due to various reasons, e.g. because of different residual solvent content of the films relative to the microspheres, differences in the polymer morphologies or, for the blends, slight differences in the relative polymer concentrations, and also because of the neglect of the imaginary part of the refractive index which is increasing towards shorter wavelengths. It has also to be kept in mind that the scattering cross section spectrum should be weighted by the PL intensity and that the

neglected imaginary part of the refractive index, although very small, leads to a spectral broadening especially towards the short wavelength edge of the spectrum. It can be seen that the theoretical and experimental modes coincide very well, which allows the identification of the resonances as TE_{l1}^{k}, or TM_{l1}^{k}, respectively, where l and k correspond to the orbital and radial orders of the modes, respectively. Because the imaginary part of the refractive index is so small in the relevant range of wavelengths that it cannot be determined by ellipsometry, the linewidths obtained from the simulation yield values for the ideal case of zero residual absorption, ideal sphericity and zero surface roughness. For example, the mode TE_{21}^{1} at 608.65 nm in the fit has a width of 0.0058 nm, corresponding to a Q factor of ≈100000. If the refractive index has an imaginary part of 10^{-5}, corresponding at this wavelength to an absorption coefficient of about 1.0 cm^{-1}, the Q factor reduces to about 60000, again for an ideal sphere of zero surface roughness. The linewidths of the sharp resonances in the experimentally obtained spectrum shown in **Figure 4**, on the other hand, are slit width limited and therefore cannot be compared to those of the fitted spectrum (for spectra acquired with higher resolution see **Figure 3**). It should be emphasized that we are discussing here the linewidths of the PL spectrum below threshold, *not* lasing linewidths

2.4. Lasing of CP Microspheres

To investigate the stimulated emission behavior of individual microspheres the latter were photoexcited by a mildly focused and attenuated pulsed Nd:YAG laser through the transparent substrate from the top of the inverted microscope, using an appropriate lens and a set of neutral density filters, respectively. **Figure 5(a,c,e,g)** displays spontaneous emission spectra under Hg lamp excitation through the objective of particular microspheres with the four compositions considered here. **Figure 5(b,d,f,h)** depicts the lasing spectra of the same microspheres, respectively, upon pulsed laser excitation. The inset figures show a zoom into the lasing line in each case. Due to the homogeneous broadening of the emission spectra of the CPs and the corresponding gain competition just a single mode of the sphere starts to produce lasing in each

case close to the lasing threshold. This is in stark contrast to a recent report on diode-pumped lasing of F8BT in **cylindrical resonators,**[61] where practically all optical resonances within the PL profile were reported to lase. The additional mode in **Figure 5h** is either due to excitation of a microsphere close to the one under investigation by reflections of the laser beam, to a

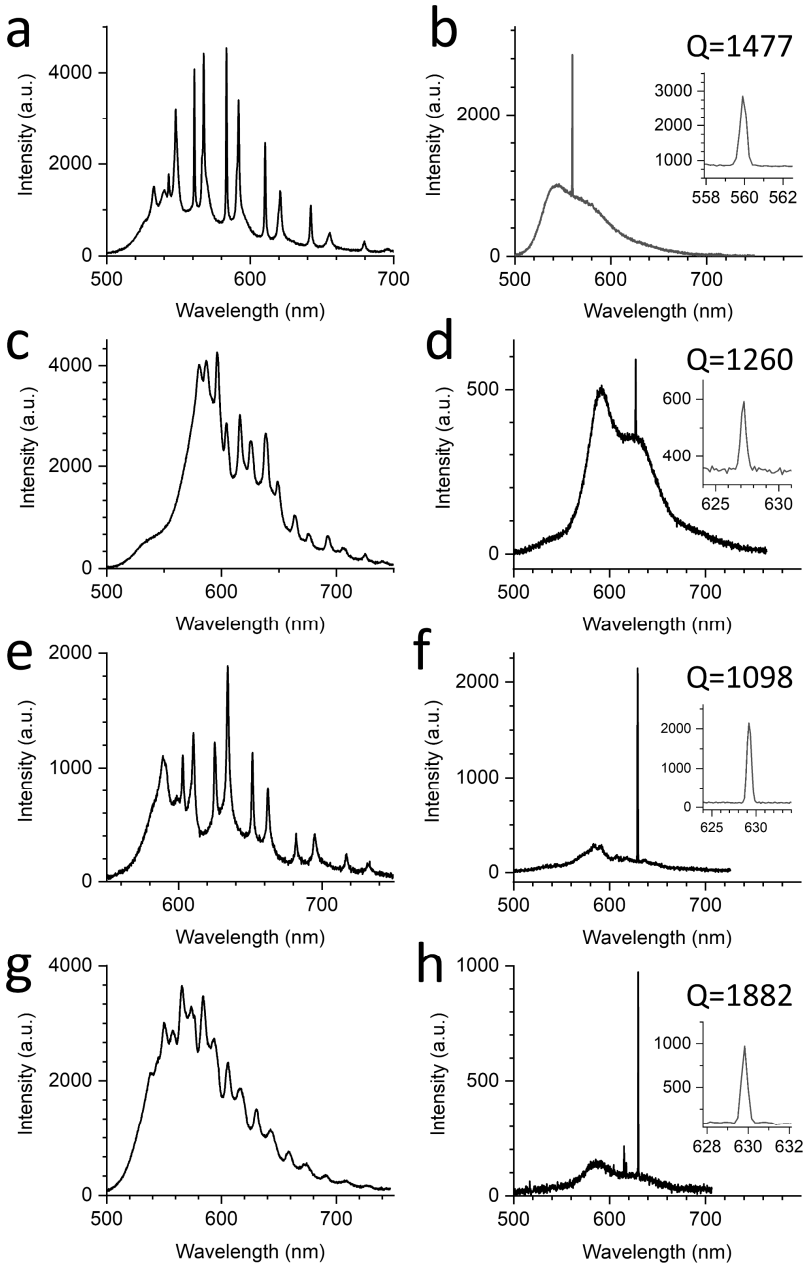

Figure 5. a) Mie resonances in spontaneous emission (figures on the left-hand side) and lasing modes (figures on the right-hand side) from the same individual microspheres. Microspheres are based on (a,b) F8BT and (c,d) 15%, (e,f) 10%, (g,h) 5% mixtures of MEH-PPV in F8BT. Graphs in the inset show expanded views of the lasing modes. Q factors are given, but are severely limited by the instrumental resolution.

deviation from sphericity, which removes the degeneracy of modes with different azimuthal mode number m, but equal orbital mode number l, or to the "spatial hole-burning effect", which arises from lasing of material in spatial regions where the main lasing mode has low intensity, for example lasing of a higher radial mode. These effects were not further studied here.

The position of that particular resonance is determined by (i) the emission intensity of that mode (ii) by the residual absorption of the CP (blend) at this wavelength (iii) FRET from F8BT to MEH-PPV. We ascribe the apparent near disappearance of the non-lasing spontaneous emission resonances in the spectra obtained with laser excitation to some heating of the microspheres due to the relatively high laser excitation powers compared to excitation by the lamp. The observed linewidths of the lasing modes are in the 0.34 to 0.57 nm range, and are severely limited by the instrumental resolution of the spectrometer coupled to the microscope. The observed lasing modes jump towards the red for the microspheres doped with MEH-PPV, compared to the spheres made from pure F8BT. Even for the lowest concentration of MEH-PPV (5%) the position of the lasing mode for the doped spheres approximately coincides with the first vibronic satellite of the emission spectrum of MEH-PPV (compare **Figure S4a**) due to the considerable residual absorption of MEH-PPV (compare **Figure S3**) at the main peak of the emission spectrum. We ascribe the observed lasing wavelengths in the doped spheres to lasing of MEH-PPV after FRET from F8BT (compare also the discussion provided above in Section 2.2). It should also be noted here that the chosen excitation wavelength for producing stimulated emission (λ = 355 nm) does not fit to the absorption of MEH-PPV (**Figure S3**), confirming once more that lasing is truly fueled by FRET.

We also studied the pump power dependence of the spontaneous PL and the lasing spectra (compare, for example, **Figure 6a**) using the experimental set-up shown in **Figure S13b** (compare the Experimental section below). As expected, the intensity of the lasing modes exhibited a clear change in slope as a function of the excitation pulse energy, whereas the width

experiences a sudden drop above the lasing threshold (**Figure 6b**). Similar results for the 5% mixture are reported in **Figure S9**.

For the quantitative determination of lasing thresholds, the microspheres were placed in a vacuum chamber as detailed in the Experimental Section. A set of 30 microspheres were studied in each case in order to obtain a statistically meaningful result. The documented thresholds (**Figure 7**) reveal significantly lower thresholds for microspheres fabricated from the mixtures than for pure F8BT, being lower by a factor of 8 for the 5% mixture. A comparison of the thresholds measured by us with previously reported results for pure F8BT and MEH-PPV, respectively, evidences a two and three orders of magnitude reduction of lasing threshold,

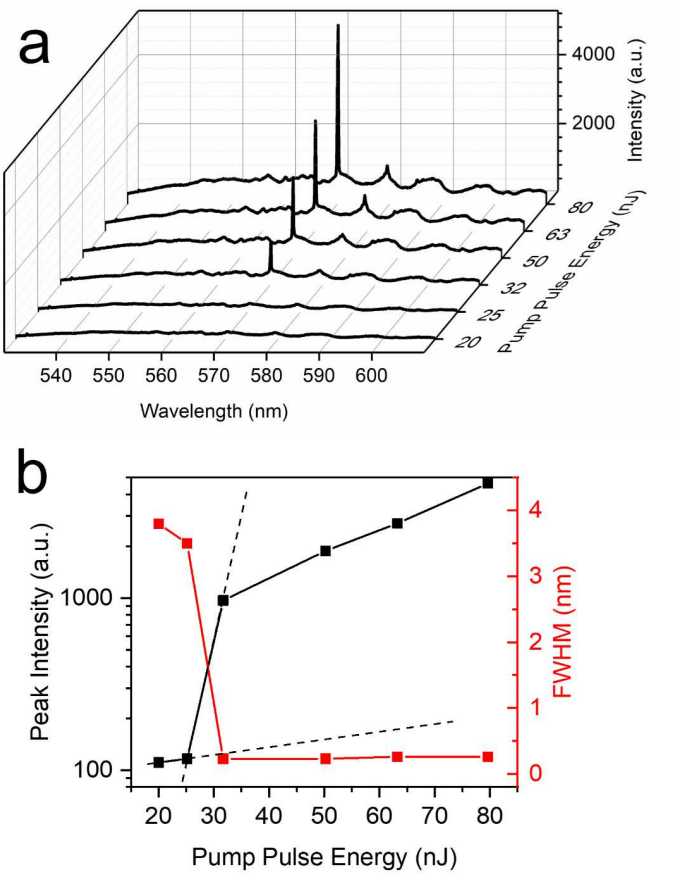

Figure 6. a) Spontaneous PL and lasing spectra of a particular F8BT microsphere and b) peak intensity and full width at half maximum (FWHM) at the 577 nm lasing line of an F8BT microsphere as a function of the energy of the pump pulse. The FWHM of the corresponding Mie resonance in the spontaneous PL spectrum is plotted below the threshold of lasing.

respectively, highlighting the beneficial role of FRET for lasing performance. This outstanding reduction in lasing thresholds is due to the significantly reduced absorption at the emission wavelength of the mixtures as well as due to the effect of MEH-PPV chain dilution in the F8BT matrix. Note that the lowest absorption at the peak of emission and the lowest lasing threshold are consistently assigned to the 5% mixture, an effect most likely due to residual absorption of the dopant itself. Our experimental result on CP microspheres differs from a recent report on lasing of organic molecules in co-crystal microcavities where FRET was not observed to reduce

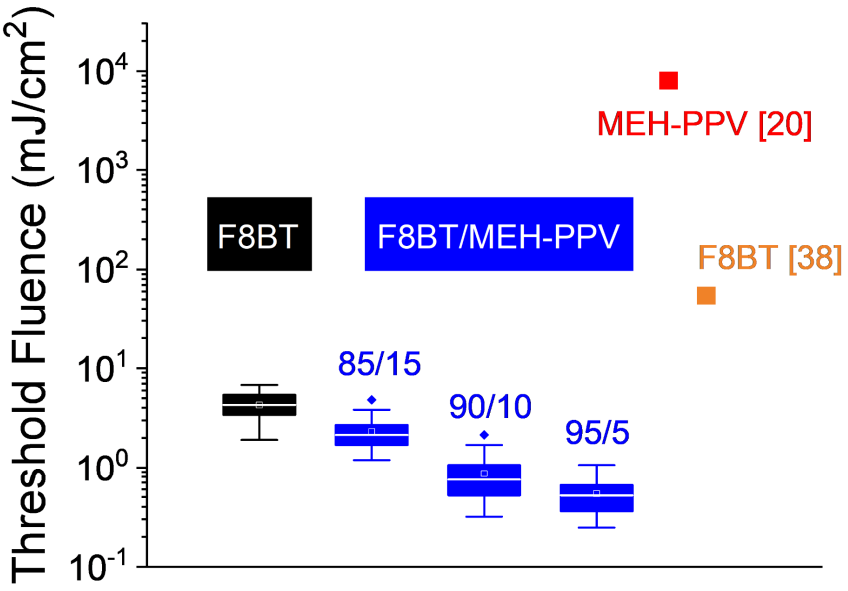

Figure 7. Statistical parameters of the distribution of threshold fluences observed for microspheres of F8BT and 5%, 10% and 15% mixtures of MEH-PPV in F8BT, respectively, and comparison of the results of this work with results previously reported for F8BT spheres (58 µJcm^{-2}) and MEH-PPV spheres (800 µJcm^{-2}).[38,20] A set of 30 microspheres were investigated in each case. Colored rectangles delimit values located in the second and third quartile, error bars mark the range of thresholds within 1.5 x interquartile range, horizontal lines stand for the median, open squares the mean and filled diamonds outliers of the measured data. Excitation conditions for the quoted literature reports: pulsed dye laser, wavelength 500 nm, pulse width 1 ns, repetition rate 20 Hz (MEH-PPV), 397 nm, 300 fs, 1 kHz (F8BT).

the lasing thresholds,[62] possibly due to a variation of the crystal quality with the different compositions.

To obtain a better estimate of the laser linewidths we operated the spectrometer of this set-up in second order of diffraction and observed linewidths still limited by the instrumental resolution (**Figures S10, S11**). However, a lower limit of the Q factor of the lasing modes of about 18000 was obtained in this way without resorting to a deconvolution with the instrumental response function (which would yield an even larger value of Q). To our knowledge, such Q value is the highest ever reported for CP microspheres The linewidth and the intensity of a particular mode as a function of the pump fluence is shown in **Figure 6b** and clearly demonstrates lasing of the microspheres.

3. Conclusion

CP microspheres based on a mixture of two CPs with outstanding lasing properties were produced by means of a microemulsions technique involving the formation of micelles from a surfactant. The obtained CP microspheres exhibit Mie resonances in spontaneous emission spectra of exceptionally high Q factors ($Q \approx 1000$ in most cases). Accordingly, we observe low lasing thresholds already for pure F8BT, significantly lower than values previously reported. Microspheres produced via the same method from F8BT:MEH-PPV blends exhibit highly efficient FRET, manifested in yellow-to-red tuning of the emission. Outstandingly, we observe an 8-fold reduction in pumping threshold with respect to microspheres produced from undoped F8BT and a three orders of magnitude lasing threshold reduction respect to the best reported value from pure MEH-PPV microspheres. Due to the homogeneous broadening of the emission only the mode with the highest gain produces lasing close to the lasing threshold. The very narrow lasing linewidths, corresponding to Q factors $Q > 18000$ in pure F8BT, the highest reported in CPs to the best of our knowledge, render our microspheres ideal for ultrasensitive sensing of any factors that affect the refractive index in the near field of the spheres, such as

gases, liquids containing variable amounts of trace agents or molecules that attach to the surface. In addition, the low lasing thresholds open the prospect of pumping CP microlasers by low-end diode lasers.

4. Experimental Section/Methods

4.1. Preparation of CP Microspheres

CTAB is dissolved in distilled water at a concentration of 0.7 mg/ml. Separately, the CPs are dissolved in $CHCl_3$ at a concentration of 22.5 mg/ml. The solutions are stirred for approximately half an hour to assure homogeneity. Subsequently, the CP solution is mixed with the aqueous solution of CTAB and agitated using a frother until homogeneity is achieved. The mixture is then transferred to an amber flask and the remaining $CHCl_3$ is left to evaporate for 24 hours. Finally, the solution is centrifuged 3 times at 2000 rpm removing the supernatant in each centrifugation. The resulting solution is deposited on quartz substrates for further investigation (**Figure S12**). Non-aggregated spheres were selected for further study.

4.2. Characterization of the Microspheres

The microsphere topographies were investigated employing an atomic force microscope (NT-MDT Ntegra) in dynamic mode. Secondary electron microscopy images of the microspheres were produced using a SEM (Carl Zeiss Sigma 300VP) operated at 1 kV. For acquisition of the PL spectra, droplets of the microsphere suspensions were deposited on a quartz substrate and allowed to dry. These samples were then placed on a home-built piezoelectric scanner on top of an inverted microscope (Nikon Eclipse Ti). The emission of individual microspheres was coupled through a dichroic beam splitter, a long pass filter and a confocal aperture to a spectrograph (ANDOR SR303i-B) equipped with a Peltier-cooled CCD (charge-coupled device, Andor Newton). PL spectra of individual microspheres could be acquired in this way under two

excitation configurations: illumination through the microscope objective (100x/0.8NA) by a high pressure mercury lamp (Osram HBO100) or excitation from the top by a frequency-tripled Nd-YAG laser (TEEM Photonics, λ = 355 nm, pulse width 300 ps) employing appropriate neutral attenuation filters (**Figure S13a**). In the latter case a reflecting microscope objective (Edmund Optics REFL OBJ 74x/0.65NA) was employed for detection in order to avoid damage to the objective. For the determination of lasing thresholds and laser linewidths the samples were placed in a vacuum recipient and excited by the focused beam of the same laser mentioned above. The emission of the microspheres was imaged onto a f = 500 mm spectrograph (Acton Research SP2500i), equipped with a 1200g/mm grating (blaze wavelength 750 nm) and a liquid nitrogen-cooled CCD (Princeton SPEX-10:400BR, **Figure S13b**). When high spectral resolution was required, e.g. for measuring Q factors significantly above 10^4, the spectrometer was operated in the second order of diffraction yielding a resolution limit corresponding to Q ≈ 18000 (compare the SI and the discussion below). The laser spot area was determined using a razor blade mounted on a micrometer-controlled xz-translation stage.

Supporting Information

Supporting Information is available from the Wiley Online Library or from the author.

The following files are available free of charge.

Supporting Information.pdf (Materials, Experimental Set-ups, Additional Spectroscopy)

Acknowledgements

The manuscript was written through contributions of all authors. All authors have given approval to the final version of the manuscript.

J.C.G. and R.W. acknowledge support by the Spanish Ministry for Science (MINECO/MICINN–FEDER projects RTI2018-097508-B-I00, PID2021-128313OB-I00) and by the Regional Government of Madrid (NMAT2D-CM). J.C.G. acknowledges a Research

Consolidation Grant (CNS2022-136191) from the Spanish Ministry of Science and Innovation. IMDEA Nanociencia acknowledges support from the 'Severo Ochoa' Programme for Centres of Excellence in R&D of the Spanish Ministry of Science and Innovation (CEX2020-001039-S). J.G.S. and S.I.V are grateful to the Ministry of Science and Innovation and Regional Government of Madrid for support through grants PEJ2018-004675-A and PEJD-2017-PRE/IND-4536. A.M.M. thankfully acknowledges a pre-doctoral grant (PIPF-2022/TEC-24494) from the Regional Government of Madrid.

Authors thank Patricia Pedraz, María Acebrón (IMDEA Nanociencia) and Francisco García Moscoso (Universidad Pablo de Olavide, Sevilla, Spain) for assistance in AFM, SEM and PL quantum yield measurements, respectively. We thank M. Campoy-Quiles (ICMAB, Barcelona, Spain) for providing us the data for the real part of the refractive index of F8BT.

Conflict of Interest

The authors declare no conflict of interest.

Data Availability Statement

The data that support the findings of this study are available from the corresponding authors upon reasonable request.

References

[1] M. L. Gorodetsky, A. A. Savchenkov, V. S. Ilchenko, *Opt. Lett.* **1996**, *21*, 453.
[2] F. Treussart, V. S. Ilchenko, J. F. Roch, P. Domokos, J. Hare, V. Lefèvre, J. M. Raimond, S. Haroche, *J. Lumin.* **1998**, *76&77*, 670.
[3] C. F. Bohren, D. R. Huffman, *Absorption and Scattering of Light by Small Particles*, John Wiley & Sons, New York, United States, **1983**.
[4] R. I. Stoian, K. V. Bui, A. T. Rosenberger, *J. Opt. (United Kingdom)* **2015**, *17*, 125011.
[5] A. Schweinsberg, S. Hocdé, N. N. Lepeshkin, R. W. Boyd, C. Chase, J. E. Fajardo, *Sensors Actuators, B Chem.* **2007**, *123*, 727.
[6] S. H. Huang, S. Sheth, E. Jain, X. Jiang, S. P. Zustiak, L. Yang, *Opt. Express* **2018**, *26*, 51.
[7] M. Gao, C. Wei, X. Lin, Y. Liu, F. Hu, Y. S. Zhao, *Chem. Commun.* **2017**, *53*, 3102.
[8] N. Toropov, G. Cabello, M. P. Serrano, R. R. Gutha, M. Rafti, F. Vollmer, *Light Sci.*

Appl. **2021**, *10*, 42.
[9] X. C. Yu, S. J. Tang, W. Liu, Y. Xu, Q. Gong, Y. L. Chen, Y. F. Xiao, *Proc. Natl. Acad. Sci. U. S. A.* **2022**, *119*, e2108678119.
[10] I. Brice, K. Grundsteins, A. Atvars, J. Alnis, R. Viter, A. Ramanavicius, *Sensors Actuators, B Chem.* **2020**, *318*, 128004.
[11] J. Liao, L. Yang, *Light Sci. Appl.* **2021**, *10*, 32.
[12] P. K. Reinis, L. Milgrave, K. Draguns, I. Brice, J. Alnis, A. Atvars, *Sensors* **2021**, *21*, 1746.
[13] Y. E. Geints, O. V. Minin, I. V. Minin, *Opt. Laser Technol.* **2022**, *151*, 108015.
[14] S. Zhang, T. Zhai, L. Cui, X. Shi, K. Ge, N. Liang, A. Hayat, *Polymers (Basel).* **2021**, *13*, 205.
[15] D. W. Vernooy, A. Furusawa, N. P. Georgiades, V. S. Ilchenko, H. J. Kimble, *Phys. Rev. A* **1998**, *57*, R2293.
[16] M. V. Artemyev, U. Woggon, R. Wannemacher, H. Jaschinski, W. Langbein, *Nano Lett.* **2001**, *1*, 309.
[17] U. Woggon, R. Wannemacher, M. V. Artemyev, B. Möller, N. Lethomas, V. Anikeyev, O. Schöps, *Appl. Phys. B Lasers Opt.* **2003**, *77*, 469.
[18] J. U. Fürst, D. V. Strekalov, D. Elser, M. Lassen, U. L. Andersen, C. Marquardt, G. Leuchs, *Phys. Rev. Lett.* **2010**, *104*, 153901.
[19] P. S. Kuo, J. Bravo-Abad, G. S. Solomon, *Nat. Commun.* **2014**, *5*, 3109.
[20] K. Gardner, M. Aghajamali, S. Vagin, J. Pille, W. Morrish, J. G. C. Veinot, B. Rieger, A. Meldrum, *Adv. Funct. Mater.* **2018**, *28*, 1802759.
[21] Z. S. Ngara, D. Okada, O. Oki, Y. Yamamoto, *Chem. – Asian J.* **2019**, *14*, 1637.
[22] J. Álvarez-Conde, E. M. García-Frutos, J. Cabanillas-Gonzalez, *Molecules* **2021**, *26*, 958.
[23] C. Wei, M. Gao, F. Hu, J. Yao, Y. S. Zhao, *Adv. Opt. Mater.* **2016**, *4*, 1009.
[24] K. Gardner, Y. Zhi, L. Tan, S. Lane, Y.-F. Xiao, A. Meldrum, *J. Opt. Soc. Am. B* **2017**, *34*, 2140.
[25] S. Ciftci, A. Mikosch, B. Haehnle, Ł. Witczak, A. J. C. Kuehne, *Chem. Commun.* **2016**, *52*, 14222.
[26] D. Yan, T. Shi, Z. Zang, S. Zhao, J. Du, Y. Leng, *Chem. Eng. J.* **2020**, *401*, 126066.
[27] S. I. Shopova, G. Farca, A. T. Rosenberger, W. M. S. Wickramanayake, N. A. Kotov, *Appl. Phys. Lett.* **2004**, *85*, 6101.
[28] J. E. Cheeney, S. T. Hsieh, N. V. Myung, E. D. Haberer, *Nanoscale* **2020**, *12*, 9873.
[29] J. Peter, C. P. G. Vallabhan, P. Radhakrishnan, V. P. N. Nampoori, M. Kailasnath, *Laser Phys.* **2013**, *23*, 115104.
[30] A. Tulek, D. Akbulut, M. Bayindir, *Appl. Phys. Lett.* **2009**, *94*, 203302.
[31] J. S. Mondragón-Ochoa, J. González-Rivera, C. Toparli, R. Khanum, R. S. Moirangthem, C. Duce, C. Ferrari, G. Barillaro, A. Erbe, *J. Phys. D. Appl. Phys.* **2022**, *55*, 055101.
[32] D. Okada, T. Nakamura, D. Braam, T. D. Dao, S. Ishii, T. Nagao, A. Lorke, T. Nabeshima, Y. Yamamoto, *ACS Nano* **2016**, *10*, 7058.
[33] D. Yu, M. Humar, K. Meserve, R. C. Bailey, S. N. Chormaic, F. Vollmer, *Nat. Rev. Methods Primers* **2021**, *1*, 83.
[34] M. Schubert, A. Steude, P. Liehm, N. M. Kronenberg, M. Karl, E. C. Campbell, S. J. Powis, M. C. Gather, *Nano Lett.* **2015**, *15*, 5647.
[35] B. Haehnle, M. Lamla, K. M. J. Sparrer, M. C. Gather, A. J. C. Kuehne, *Adv. Opt. Mater.* **2021**, *9*, 2001553.
[36] D. Braam, S. Kushida, R. Niemöller, G. M. Prinz, H. Saito, T. Kanbara, J. Kuwabara, Y. Yamamoto, A. Lorke, *Sci. Rep.* **2016**, *6*, 19635.
[37] Y. Yamamoto, *Polym. J.* **2016**, *48*, 1045.

[38] S. Kushida, D. Okada, F. Sasaki, Z. H. Lin, J. S. Huang, Y. Yamamoto, *Adv. Opt. Mater.* **2017**, *5*, 1700123.
[39] S. Kushida, D. Braam, T. D. Dao, H. Saito, K. Shibasaki, S. Ishii, T. Nagao, A. Saeki, J. Kuwabara, T. Kanbara, M. Kijima, A. Lorke, Y. Yamamoto, *ACS Nano* **2016**, *10*, 5543.
[40] Y. S. L. V. Narayana, D. Venkatakrishnarao, A. Biswas, M. A. Mohiddon, N. Viswanathan, R. Chandrasekar, *ACS Appl. Mater. Interfaces* **2016**, *8*, 952.
[41] Y.-J. Lin, H.-Y. Chiang, O. Oki, S. Kushida, S.-W. Chang, S.-T. Chiu, Y. Yamamoto, T. Hosokai, M. Horie, *ACS Appl. Polym. Mater.* **2019**, *1*, 2240.
[42] S. Kushida, D. Braam, C. Pan, T. D. Dao, K. Tabata, K. Sugiyasu, M. Takeuchi, S. Ishii, T. Nagao, A. Lorke, Y. Yamamoto, *Macromolecules* **2015**, *48*, 3928.
[43] C. Sun, M. M. Mróz, J. R. Castro Smirnov, L. Lüer, D. Hermida-Merino, C. Zhao, M. Takeuchi, K. Sugiyasu, J. Cabanillas-González, *J. Mater. Chem. C* **2018**, *6*, 6591.
[44] L. Bai, C. Sun, Y. Han, C. Wei, X. An, L. Sun, N. Sun, M. Yu, K. Zhang, J. Lin, M. Xu, L. Xie, H. Ling, J. Cabanillas-Gonzalez, L. Song, X. Hao, W. Huang, *Adv. Opt. Mater.* **2020**, *8*, 1901616.
[45] J. Royakkers, A. Minotto, D. G. Congrave, W. Zeng, A. Hassan, A. Leventis, F. Cacialli, H. Bronstein, *Chem. Mater.* **2020**, *32*, 10140.
[46] J. Lin, B. Liu, M. Yu, X. Wang, Z. Lin, X. Zhang, C. Sun, J. Cabanillas-Gonzalez, L. Xie, F. Liu, C. Ou, L. Bai, Y. Han, M. Xu, W. Zhu, T. A. Smith, P. N. Stavrinou, D. D. C. Bradley, W. Huang, *Adv. Mater.* **2019**, *31*, 1804811.
[47] D. Sahoo, K. Sugiyasu, Y. Tian, M. Takeuchi, I. G. Scheblykin, *Chem. Mater.* **2014**, *26*, 4867.
[48] Z. Yu, X. Guo, Q. Zhang, L. Chi, T. Chen, R. Xia, L. Wu, L. Lüer, J. Cabanillas-Gonzalez, *J. Phys. Chem. C* **2016**, *120*, 11350.
[49] J. R. C. Smirnov, Q. Zhang, R. Wannemacher, L. Wu, S. Casado, R. Xia, I. Rodriguez, J. Cabanillas-González, *Sci. Rep.* **2016**, *6*, 34565.
[50] M. Mamada, R. Komatsu, C. Adachi, *ACS Appl. Mater. Interfaces* **2020**, *12*, 28383.
[51] J. R. C. Smirnov, A. Sousaraei, M. R. Osorio, S. Casado, J. J. Hernández, L. Wu, Q. Zhang, R. Xia, D. Granados, R. Wannemacher, I. Rodriguez, J. Cabanillas-Gonzalez, *npj Flex. Electron.* **2019**, *3*, 17.
[52] G. Canazza, F. Scotognella, G. Lanzani, S. De Silvestri, M. Zavelani-Rossi, D. Comoretto, *Laser Phys. Lett.* **2014**, *11*, 035804.
[53] Q. Zhang, Q. Wei, X. Guo, G. Hai, H. Sun, J. Li, R. Xia, Y. Qian, S. Casado, J. R. Castro-Smirnov, J. Cabanillas-Gonzalez, *Adv. Sci.* **2019**, *6*, 1801455.
[54] Q. Zhang, J. Liu, Q. Wei, X. Guo, Y. Xu, R. Xia, L. Xie, Y. Qian, C. Sun, L. Lüer, J. Cabanillas-Gonzalez, D. D. C. Bradley, W. Huang, *Adv. Funct. Mater.* **2018**, *28*, 1705824.
[55] M. Ibisate, J. F. Galisteo-López, V. Esteso, C. López, *Adv. Opt. Mater.* **2013**, *1*, 651.
[56] X. Tang, Y. T. Lee, Z. Feng, S. Y. Ko, J. W. Wu, V. Placide, J. C. Ribierre, A. D'Aléo, C. Adachi, *ACS Mater. Lett.* **2020**, *2*, 1567.
[57] C. Sun, L. Bai, J. C. Roldao, A. Burgos-Caminal, O. Borrell-Grueiro, J. Lin, W. Huang, J. Gierschner, W. Gawelda, L. Bañares, J. Cabanillas-González, *Adv. Funct. Mater.* **2022**, *32*, 2206723.
[58] Y. Zhi, Z. Feng, T. Mehreen, X. Liu, K. Gardner, X. Li, B. O. Guan, L. Zhang, S. I. Vagin, B. Rieger, A. Meldrum, *Inorganics* **2022**, *10*, 101.
[59] J. S. Chen, A. Dasgupta, D. J. Morrow, R. Emmanuele, T. J. Marks, M. C. Hersam, X. Ma, *ACS Nano* **2022**, *16*, 16776.
[60] P. N. Stavrinou, G. Ryu, M. Campoy-Quiles, D. D. C. Bradley, *J. Phys.: Condens. Matter* **2007**, *19*, 466107.
[61] B. Niu, X. Shi, K. Ge, J. Ruan, Z. Xu, S. Zhang, D. Guo, T. Zhai, *Nanoscale Adv.*

2022, *4*, 2153.
[62] D. Okada, S. Azzini, H. Nishioka, A. Ichimura, H. Tsuji, E. Nakamura, F. Sasaki, C. Genet, T. W. Ebbesen, Y. Yamamoto, *Nano Lett.* **2018**, *18*, 4396.

ABBREVIATIONS

CP: Conjugated Polymer; F8BT: Poly[(9,9-di-*n*-octylfluorenyl-2,7-diyl)-*alt*-(benzo[2,1,3]thiadiazol-4,8-diyl)]; MEH-PPV: Poly[2-methoxy-5-(2'-ethylhexyloxy)-1,4-phenylene vinylene; CTAB: Cetyl(trimethyl)ammonium Bromide, FRET: Förster Resonant Energy Transfer; Nd:YAG: Neodymium-doped Yttrium Aluminium Garnet; PL: Photoluminescence; AFM: Atomic Force Microscopy; f: Focal length; SEM: Scanning Electron Microscopy; ASE: Amplified Stimulated Emission; CCD: Charge-coupled Device; Ra: average roughness; RMS: Root mean square; rpm: Revolutions per minute; TE: Transverse Electric; TM: Transverse Magnetic; UV-Vis: Ultraviolet-Visible